AD-A086 218 CALIFORNIA RESEARCH AND TECHNOLOGY INC WOODLAND HILLS F/G 18/3
EFFECTS OF DEBRIS ENTRAINMENT AND MULTI-PHASE FLOW ON PLUG LOAD--ETC(U)
SEP 78 M ROSENBLATT, G E CARPENTER DNA001-77-C-0239
UNCLASSIFIED CRT-3150F DNA-4686F NL

1 OF 1
AD
A086218

END
DATE
FILMED
8-80
DTIC

(10) LEVEL II

AD-E300809

DNA 4686F

EFFECTS OF DEBRIS ENTRAINMENT AND MULTI-PHASE FLOW ON PLUG LOADING IN AN MX TRENCH

ADA086218

California Research & Technology, Inc.
6269 Variel Avenue
Woodland Hills, California 91367

15 September 1978

Final Report for Period 1 May 1977—31 October 1977

CONTRACT No. DNA 001-77-C-0239

APPROVED FOR PUBLIC RELEASE;
DISTRIBUTION UNLIMITED.

DDC FILE COPY

THIS WORK SPONSORED BY THE DEFENSE NUCLEAR AGENCY
UNDER RDT&E RMSS CODE B344077462 J24AAXYX95502 H2590D.

DTIC
ELECTE
JUL 8 1980
S D
B

Prepared for
Director
DEFENSE NUCLEAR AGENCY
Washington, D. C. 20305

80 4 8 005

Destroy this report when it is no longer needed. Do not return to sender.

PLEASE NOTIFY THE DEFENSE NUCLEAR AGENCY, ATTN: STTI, WASHINGTON, D.C. 20305, IF YOUR ADDRESS IS INCORRECT, IF YOU WISH TO BE DELETED FROM THE DISTRIBUTION LIST, OR IF THE ADDRESSEE IS NO LONGER EMPLOYED BY YOUR ORGANIZATION.

UNCLASSIFIED

SECURITY CLASSIFICATION OF THIS PAGE (When Data Entered)

REPORT DOCUMENTATION PAGE

READ INSTRUCTIONS BEFORE COMPLETING FORM

1. REPORT NUMBER: DNA 4686F

2. GOVT ACCESSION NO.: AD-A086 218

3. RECIPIENT'S CATALOG NUMBER:

4. TITLE (and Subtitle): EFFECTS OF DEBRIS ENTRAINMENT AND MULTI-PHASE FLOW ON PLUG LOADING IN AN MX TRENCH.

5. TYPE OF REPORT & PERIOD COVERED: Final Report, for Period 1 May 1977—31 October 1977

6. PERFORMING ORG. REPORT NUMBER: 3150F

7. AUTHOR(s):
Martin Rosenblatt
Gene E. Carpenter
Robert P. Bilyeu

8. CONTRACT OR GRANT NUMBER(s): DNA 001-77-C-0239

9. PERFORMING ORGANIZATION NAME AND ADDRESS:
California Research & Technology, Inc.
6269 Variel Avenue
Woodland Hills, California 91367

10. PROGRAM ELEMENT, PROJECT, TASK AREA & WORK UNIT NUMBERS: Subtask J24AAXYX955-02

11. CONTROLLING OFFICE NAME AND ADDRESS:
Director
Defense Nuclear Agency
Washington, D.C. 20305

12. REPORT DATE: 15 September 1978

13. NUMBER OF PAGES: 44

14. MONITORING AGENCY NAME & ADDRESS (if different from Controlling Office):

15. SECURITY CLASS (of this report): UNCLASSIFIED

15a. DECLASSIFICATION/DOWNGRADING SCHEDULE

16. DISTRIBUTION STATEMENT (of this Report):
Approved for public release; distribution unlimited.

17. DISTRIBUTION STATEMENT (of the abstract entered in Block 20, if different from Report)

18. SUPPLEMENTARY NOTES
This work sponsored by the Defense Nuclear Agency under RDT&E RMSS Code B344077462 J24AAXYX95502 H2590D.

19. KEY WORDS (Continue on reverse side if necessary and identify by block number)
MX
Multi-phase Flow
Mixtures
Trench Wall Ablation
Debris Entrainment
Uncertainties

20. ABSTRACT (Continue on reverse side if necessary and identify by block number)
The $1\frac{1}{2}$-D version of the multi-phase DICE code was used to analyze the flow of hot air and wall debris in covered MX trenches after an on-line burst. In DICE, debris particles are coupled to the air flow by thermal and drag mechanisms. The objective was to examine the effects of major uncertainties in the timing and magnitude of wall removal and debris entrainment upon the pressure and impulse loading on a rigid plug in the trench. The contributions to impulse due both to pressure loading and the momentum of the debris mass were considered.

DD FORM 1 JAN 73 1473 EDITION OF 1 NOV 65 IS OBSOLETE

371 223

UNCLASSIFIED

SECURITY CLASSIFICATION OF THIS PAGE (When Data Entered)

20. ABSTRACT (Continued)

Transfer of momentum and energy from the hot gas flow to the debris attenuates pressures and velocities. In all cases treated, the maximum pressure and impulse calculated on the plug were substantially lower than would be the case if no debris were present (i.e., if the flow in the trench consisted only of hot air). Where debris mass became entrained near the shock (say within 20-50 feet after the shock passes), plug loading was reduced by orders of magnitude. For example, entrainment of the debris from 0.15-in. of wall recession (with entrainment starting 18 feet behind the shock) reduced the maximum pressure on the plug from 6800 to 78 bars and the impulse from 24 to 3 bar-sec (as compared to air-only flow in the trench). Techniques to enhance early entrainment would be useful in reducing the design load on plugs. Debris not entrained until 100 feet or more behind the shock front has a much smaller effect on plug loading.

It is concluded that entrainment of debris from a modest thickness of wall recession into the flow in the trench can reduce the loading on a rigid plug in the tunnel by orders of magnitude, but this effect is quite sensitive to uncertainties in the entrainment processes.

TABLE OF CONTENTS

Section		Page
I.	INTRODUCTION AND SUMMARY	5
	1.1 Background and Objectives	5
	1.2 Approach	6
	1.3 Summary and Conclusions	8
II.	ENTRAINMENT MODEL	12
III.	PLUG LOADING	14
	3.1 Effects of Entrainment Delay and Mass Loading	14
	3.2 Effects of Particle Size	21
IV.	IN-TRENCH RESPONSE	24
	4.1 Shock Pressure Attenuation	24
	4.2 Wall Recession	25
APPENDIX A -	PHYSICAL MODELS USED IN 1½-D DICE CALCULATIONS	31
	A.1 Aerodynamic Drag	32
	A.2 Thermal Interaction	32
	A.3 1½-D Venting and Wall Expansion	33
REFERENCES		38

ACCESSION for
NTIS White Section ☑
DDC Buff Section ☐
UNANNOUNCED ☐
JUSTIFICATION
BY
DISTRIBUTION/AVAILABILITY CODES
Dist. AVAIL. and/or SPECIAL
A

LIST OF ILLUSTRATIONS

Figure		Page
1.	Processes Treated in 1½-D DICE Solutions.	7
2.	Pressure-Time Histories on the Plug for Variations in the Mass Entrainment Parameter, $\beta(x)=\dot{T}/U_g$. . . .	11
3.	Mass Entrainment Parameter, β, versus Distance Behind Shock Front, x	16
4.	Maximum Pressure and Impulse Delivered to the Plug for Variations in Mass Entrainment Parameter, $\beta=\beta(x)$	17
5.	Maximum Impulse (I_M) and Shock Time of Arrival (TOA) versus Maximum Pressure (P_M) at the Plug for Cases 1 through 6	18
6.	A Comparison of Pressure and Impulse Time Histories using Two Wall Debris Entrainment Models.	20
7.	Time Histories of Pressure Delivered to the Plug and Impulse for Variations in the Particle Size Distribution.	22
8.	Shock Pressure vs Distance Attenuation Curves for the L=18 ft (Case 10) and L=108 ft (Case 2) Cases using a Step Entrainment Function with $\bar{\beta}=10^{-3}$ . . .	26
9.	Shock Pressure vs Distance for Various Wall Debris Entrainment Parameters, $\bar{\beta}$=.01, .001, and .0001. . .	27
10.	Shock Pressure Attenuation with Distance for Variations in Entrained Particle Size Distribution.	28
11a.	Wall Recession vs Distance Profiles for $\bar{\beta}=10^{-3}$ and $\bar{\beta}=10^{-4}$	29
11b.	Wall Recession vs Distance Profiles with Entrained Particle Distributions of D_p = .01 cm and D_p = .1, 1, and 10 cm.	29
12.	Extinction Times versus Particle Diameter for Radiative and Convective Heat Transfer Assuming a Small Dirt to Air Mass Ratio.	34

LIST OF ILLUSTRATIONS (Cont'd)

Figure		Page
13a.	Equivalence of Circular and Square Trench Cross-sections	35
13b.	Wall Expansion and Venting of Equivalent Square Trench	35

LIST OF TABLES

Table		Page
1.	Maximum Pressures and Impulses Delivered to Plug for Variations in Debris Entrainment Model	15
2.	Maximum Pressures and Impulses Delivered to the Plug for Variations in Particle Size Distribution and Thermal Interaction	23

PRECEDING PAGE BLANK - NOT FILMED

SECTION I

INTRODUCTION AND SUMMARY

1.1 BACKGROUND AND OBJECTIVES

The survivablility of any candidate M-X basing system must be evaluated using estimates of the hostile environment produced by nuclear bursts. Experimental and/or numerical simulations can be used to predict the physical characteristics of the hostile environment. These predictions and their associated uncertainties can then be used in analysis of the structural response of important elements in the basing system.

This report is concerned with one of the physical processes which affects the design environment in the buried-trench multiple aim point (MAP) basing concept[1]: After a nuclear burst within the trench or on the surface above a trench, a strong shock will be driven down the trench. The high velocity flow of shocked air in the trench will vaporize, melt, crush, and mix trench wall material (e.g., concrete, soil). Much of the debris* will interact and become entrained into the flow, and this debris will attenuate the air flow velocity and shock strength by absorbing momentum and energy through drag and heat exchange. Our objective has been to examine the degree of this attenuation and the effects of debris entrainment (*and associated uncertainties*) on the pressure and impulse** delivered to the plug in an MX trench.

---

* We will use the term "debris" to include both vapor and condensed phase trench materials which become entrained into the high temperature air flow.

** Impulse is delivered to the plug both by air pressure and by debris impact, i.e.,

$$I = \int_0^t P dt + \frac{\Sigma M_d U_d}{A}$$

1.2 APPROACH

The 1½-D version of the multi-phase DICE code* was used to analyze the flow of hot air and debris in covered MX trenches, and to examine the effects of debris entrainment upon the loading imposed on a rigid plug in the trench 1800 feet from a 1 Mt on-line surface burst. For all the cases which were analyzed, it was assumed that the burst coupled 6.2 kt (all internal energy) to the air in the trench in the first 18 feet in both directions from the burst (i.e., 3.1 kt on each side). A 14 foot diameter trench buried 6 feet in the ground is the assumed configuration.

These 1½-D numerical simulations treated or took into consideration the phenomena which are shown in Figure 1, either through explicit calculations of the physical processes, or through prescription by separate models.

The processes by which material is removed from the trench wall and becomes entrained in the flow in the trench involve complex stress wave, thermodynamic, and turbulent boundary layer and mixing phenomena occurring under conditions which have not been accessible to experimental observation or investigation. Consequently there are major uncertainties, for any trench materials or construction, in the mass flux of debris off the walls, in the physical state of the debris (including size distribution of condensed-phase material), and in the timing of effective entrainment (mixing) of debris into the trench flow.

---

* The basic DICE code[2,3] is a 2-D (axisymmetric) method to model the dynamics of formation of dust clouds following nuclear surface bursts. It is an implicit, compressible, Eulerian finite difference code which can treat the separate flow of different phases (condensed and vapor), material species, and particle sizes. The different groups and the basic medium (usually air) are mutually coupled by aerodynamic (drag) and thermodynamic (heat exchange) processes.

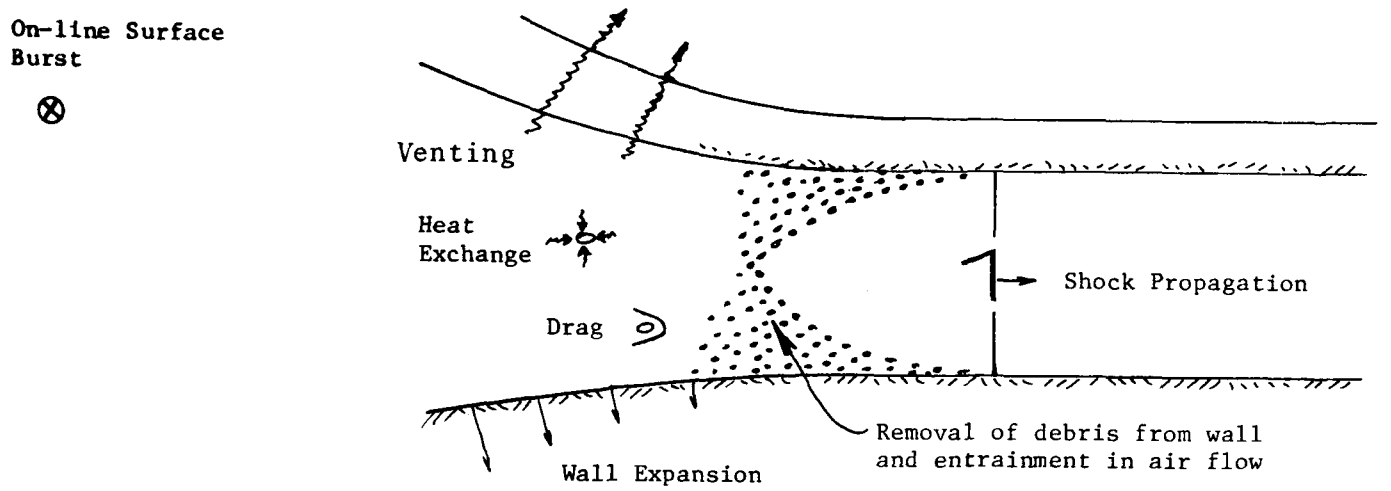

Processes treated explicitly	Processes prescribed by separate models	Processes not treated
Shock generation and propagation in tunnel, and reflection from rigid plug	Debris removal from trench walls by ablation, scouring, crushing, etc.	Turbulent mixing (except as crudely treated by varying nature of entrainment model)
Hot air flow	Debris particle sizes	Wall friction
Aerodynamic drag between debris and air flow	Debris entrainment into air flow	Surface air blast
Heat exchange between debris and hot air	Trench wall expansion	Individual debris particle impacts on plug
Melting and ablation of debris	Venting	
Transfer of debris momentum to plug		

Figure 1. Processes Treated in 1½-D DICE Solutions.

In the current program, we examined the *effects* of these uncertainties on pressure attenuation, trench wall recession, and the plug environment. This was done by numerical simulations in which several substantially different models were prescribed for the mass flux of debris, its size distribution, and the timing of its entry into the trench flow.

1.3 SUMMARY AND CONCLUSION

A baseline solution of the trench air flow with *no debris* (air-only) produced a maximum pressure of 6800 bars on the plug, and an impulse of 24 bar-sec. Eleven calculations were made of the trench flow with various debris entrainment models. In all cases, the maximum pressure, and the impulse on the plug (which includes the contributions of both pressure loading and debris mass) were substantially lower than in the air-only case. However, the magnitude of the reductions was strongly affected by the entrainment parameters.

Three aspects of debris entrainment were examined:

- <u>Entrainment delay (mixing length)</u>. Wall removal at a given station in the trench begins as soon as the shock passes. However, some interval of time (and therefore of distance behind the shock) elapses before debris is mixed with the flow over the entire cross-sectional area of the trench. To take this delay into consideration, we used the entrainment models in the following sketch to prescribe the behavior of the wall recession thickness, T, as a function of local gas flow velocity, Ug, and the distance behind the shock front, X.

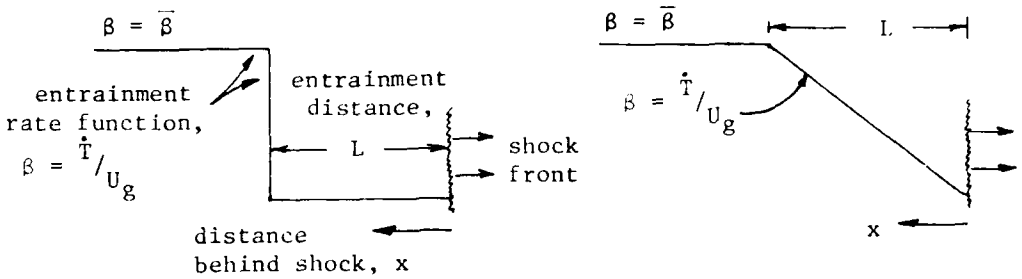

Delayed-Step Entrainment

Ramp Entrainment

$\dot{T} = \beta(x)\, U_g$ is the wall recession rate from debris entrainment

The entrainment rate parameter, $\bar{\beta}$, is the maximum ratio of wall recession rate, $\dot{T}$, to the *local* velocity of the gas flow, U_g.

Plug loading was found to be very sensitive to the entrainment delay. Where significant entrainment occurred near the shock (say 20-50 feet behind the shock), plug loading was reduced by orders of magnitude. For example entrainment of the debris from 0.15-in. of wall recession (with entrainment starting 18 feet behind the shock) reduced the maximum pressure on the plug from 6800 bars to 78 bars and the impulse from 24 to 3 bar-sec (as compared to the air-only case).

- Entrainment rate (and entrained mass). Increasing the entrainment rate (and mass) reduces loading on the plug; it may be possible to effectively quench the gas flow through techniques which enhance entrainment *within say 20-50 feet behind the shock.*

Figure 2 shows the effects of entrainment delay (mixing length) and the entrainment rate function, $\beta = \dot{T}/U_g$, on the pressure-time history at the plug for several cases. The important effects of an order of magnitude increase in the entrainment rate parameter can be seen by comparing Cases 3 and 5. Similarly, the effects of reducing the entrainment distance by a factor of two (from 108 to 54 feet) can be appreciated by comparing Case 5 to Case 6.

- Debris size. Analysis in which the debris mass is initially divided evenly between 0.1, 1, and 10 cm particles were compared with cases using just .01 cm (= 100μ) particles. The smaller distribution reduced plug peak pressure loading by about a factor of 5 more than the larger distribution. Both drag and heat transfer depend on particle size; to determine which is more important, some analyses were repeated with *no* heat transfer being allowed between the gas and the particles. Plug loading was essentially the same, *with or without heat transfer*. This indicates that the addition of debris mass affects the mixed-phase flow dynamics primarily through drag interactions rather than through thermal interactions.

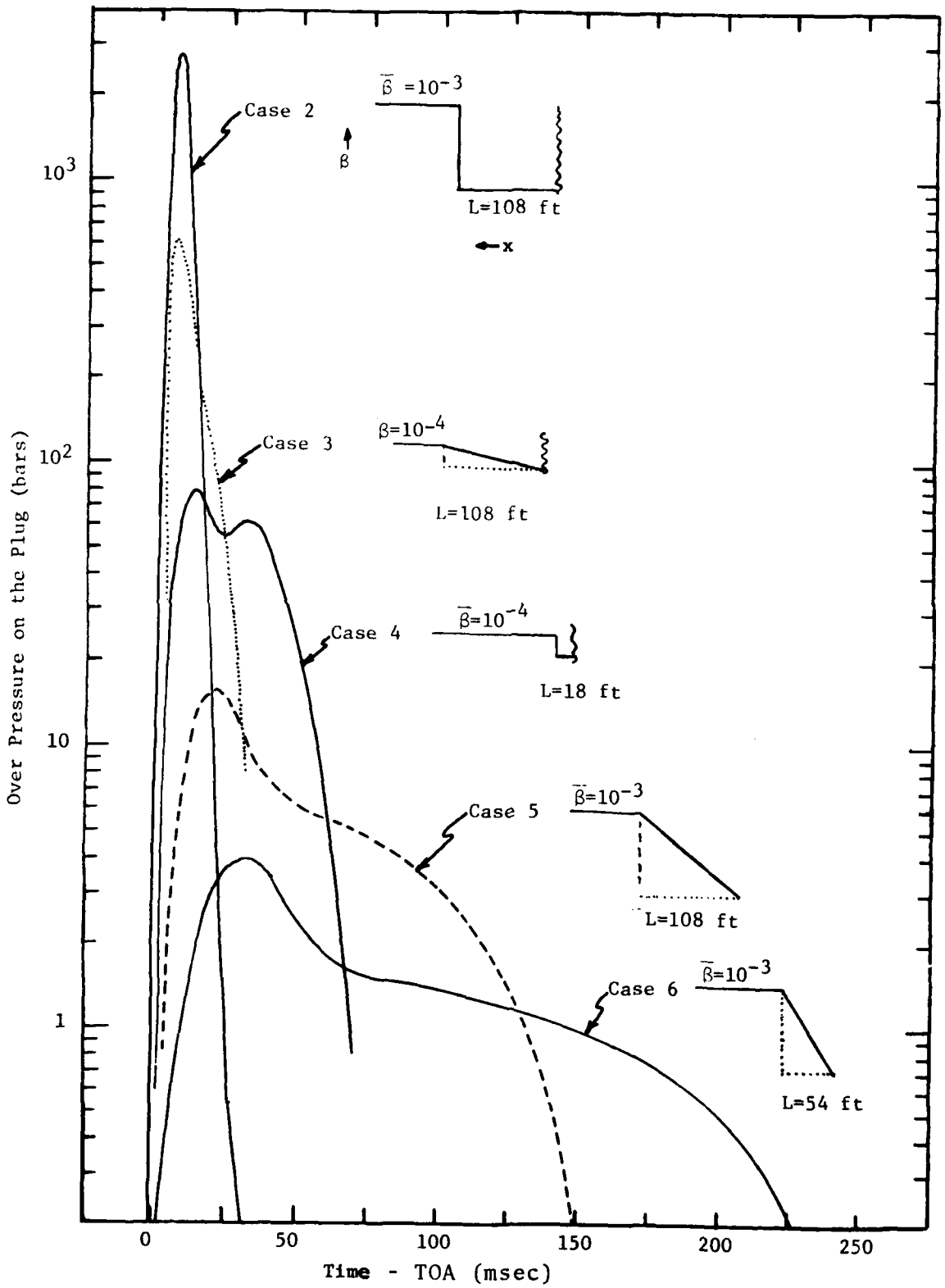

Figure 2. Pressure-Time Histories on the Plug for Variations in the Mass Entrainment Parameter, $\beta(x) = \dot{T}/U_g$.

SECTION II

ENTRAINMENT MODEL

In the multi-phase DICE analyses, passage of the air shock is assumed to initiate removal of wall material and to start its mixing with the air flow. Debris is assumed to be solid-phase silica at the time of mixing, but thermal interactions can subsequently melt and vaporize the particles. The initial debris particle size is specified (sizes from 100μ to 10 cm were considered). The entrainment delay and mass rate are specified by the following models:

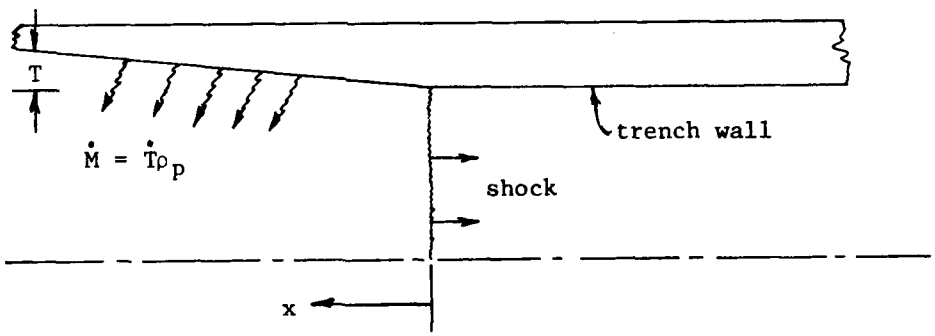

T = wall recession

x = distance behind shock

ρ_p = 2 g/cm^3 = trench wall material density

$\dot{M}$ = mass entrainment rate <u>per unit area</u> at any trench station

$$= \dot{T}\rho_p = \beta\rho_p U_g$$

where $\beta = \dfrac{\dot{T}}{U_g} \equiv$ entrainment rate parameter which is a function of x

U_g = local gas flow velocity

Note that both β and U_g are functions of the instantaneous distance of the trench station behind the shock front.

The variation of β with x was described by delayed step-function models and by ramp-function models. The parameters for several of the models used are shown in Figure 3, page 15.

The variation of U_g with x depends on the flow dynamics behind the shock. These flow dynamics are affected by the entrainment of debris; hence U_g is coupled to the entrainment delay and the entrainment mass rate, $\dot{M}$. This coupling is taken into consideration explicitly in the numerical calculations.

Models used in the DICE calculations for other processes, including aerodynamic drag, thermal interactions, and simulation of tunnel wall expansion and venting, are described in the Appendix.

SECTION III

PLUG LOADING

3.1 EFFECTS OF ENTRAINMENT DELAY AND MASS LOADING

Table 1 summarizes the time of arrival, maximum pressure, (P_M) and impulse (I_M) delivered to the plug for six variations in wall debris entrainment characteristics. Case 1, the limiting case with no debris (air only), was run for comparison*. Cases 2 through 6 use the *entrainment rate parameters* $\beta(x)$, shown on Figure 3. Figure 4 lists the maximum pressures and impulses directly on the $\beta(x)$ profiles, in order to illustrate the sensitivity of P_M and I_M to uncertainties in debris entrainment.

A comparison of the two delayed step-function cases (2 and 4) shows that introducing mass near the shock front is very effective in attenuating the plug P_M and I_M. When the "mixing length" (L in Table 1) was reduced from 108 feet to 18 feet, the peak pressure on the plug dropped from 2500 bars to 78 bars (factor of 32) and the impulse dropped from 12 bar-sec to 3 bar-sec (factor of 4). Similarly, results when ramp functions of β were used (Cases 3,5, and 6) show a strong dependence on the debris entrainment characteristics near the shock front.

Figure 5 is a plot of impulse and time of arrival versus maximum pressure on the plug for Cases 1 through 6. The impulse delivered to the plug varies roughly with the .6 power of maximum pressure, $I_M \sim (P_M)^{.6}$, and the time of arrival varies roughly with the ~.3 power, $TOA \sim (P_M)^{-.3}$. The generality of these relationships is not known. However, if validated, these are significant

---

* Results from the MARVEL test (2.1 kt burst in a 3.2-foot dia. tunnel) have shown that the air-only model is a poor representation of what actually happens. Some incorporation of wall ablation and scouring is needed to explain the MARVEL observations.

Table 1. Maximum Pressures and Impulses Delivered to Plug for Variations in Debris Entrainment Model.

Case	Entrainment Model $\beta=\beta(x)=\dot{T}/U_g$	Parameters		Plug Loading		
		$\bar{\beta}$	L (ft)	TOA (msec)	P_M (bars)	I_M (bar-sec)
1	Air Only (no debris)	-	-	26	6800	24
2	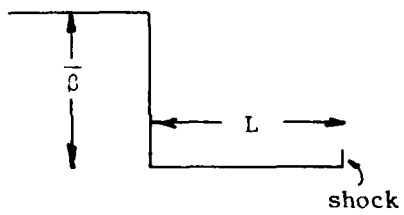	10^{-3}	108	29	2500	12
3		10^{-4}	108	42	621	6
4	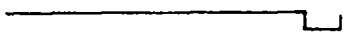	10^{-4}	18	81	78	3
5		10^{-3}	108	140	16	0.8
6	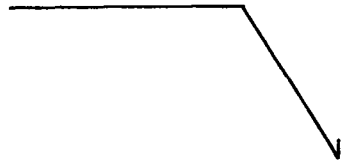	10^{-3}	54	240	4	0.3

In all these debris models, total mass was initially divided equally between 0.1, 1, and 10 cm particles.

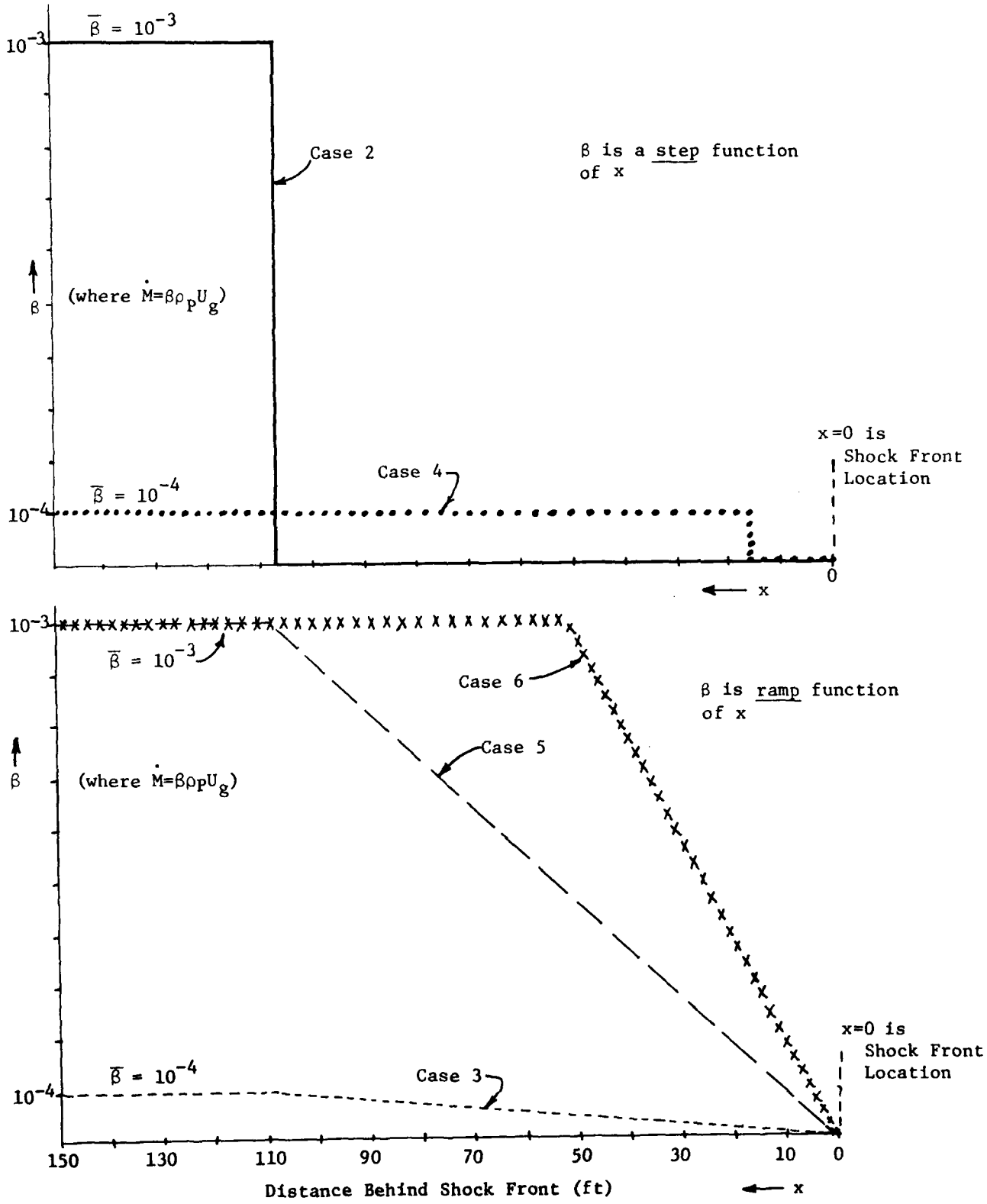

Figure 3. Mass Entrainment Parameter, β, versus Distance Behind Shock Front, x.

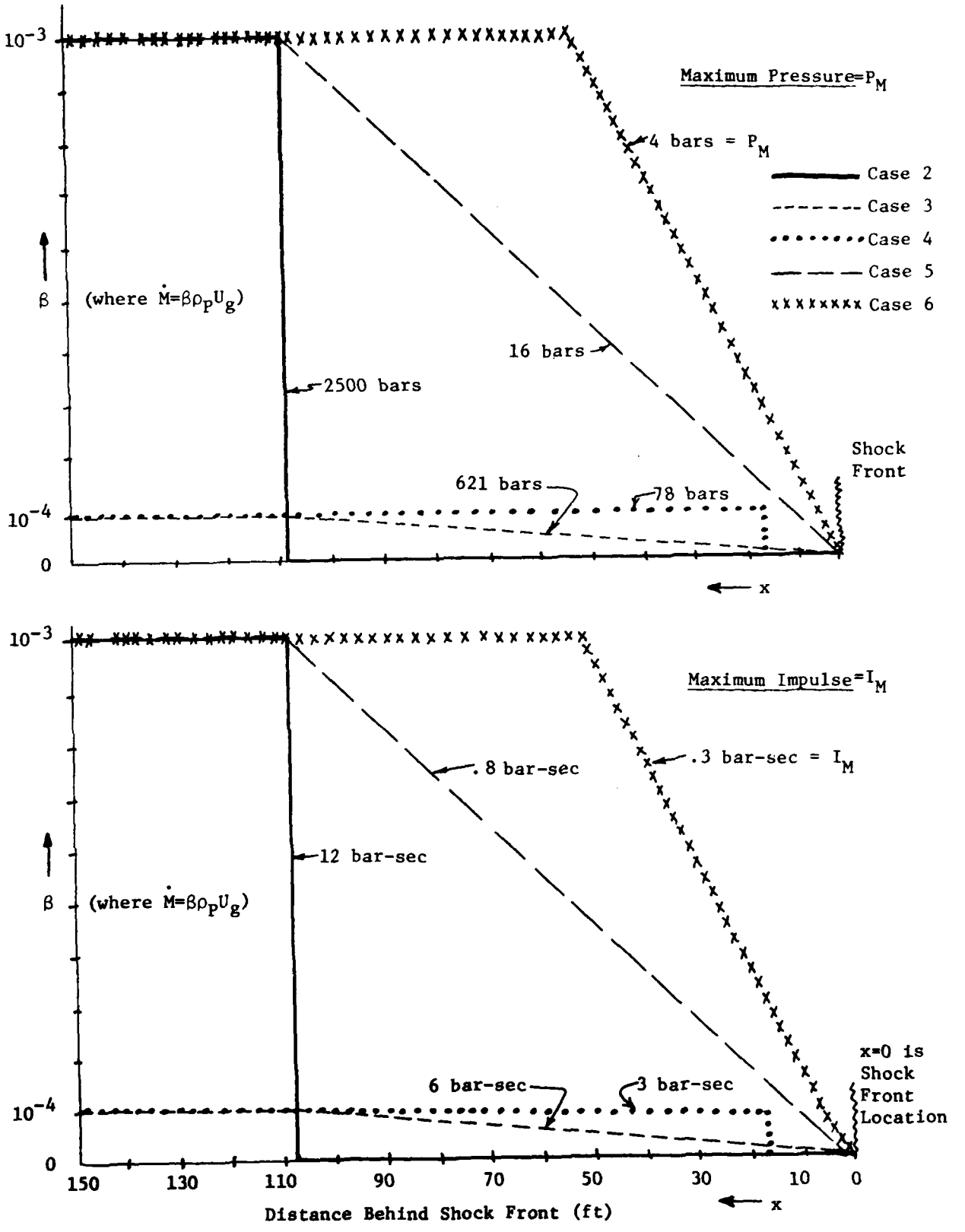

Figure 4. Maximum Pressure and Impulse Delivered to the Plug for Variations in Mass Entrainment Parameter, $\beta = \beta(x)$.

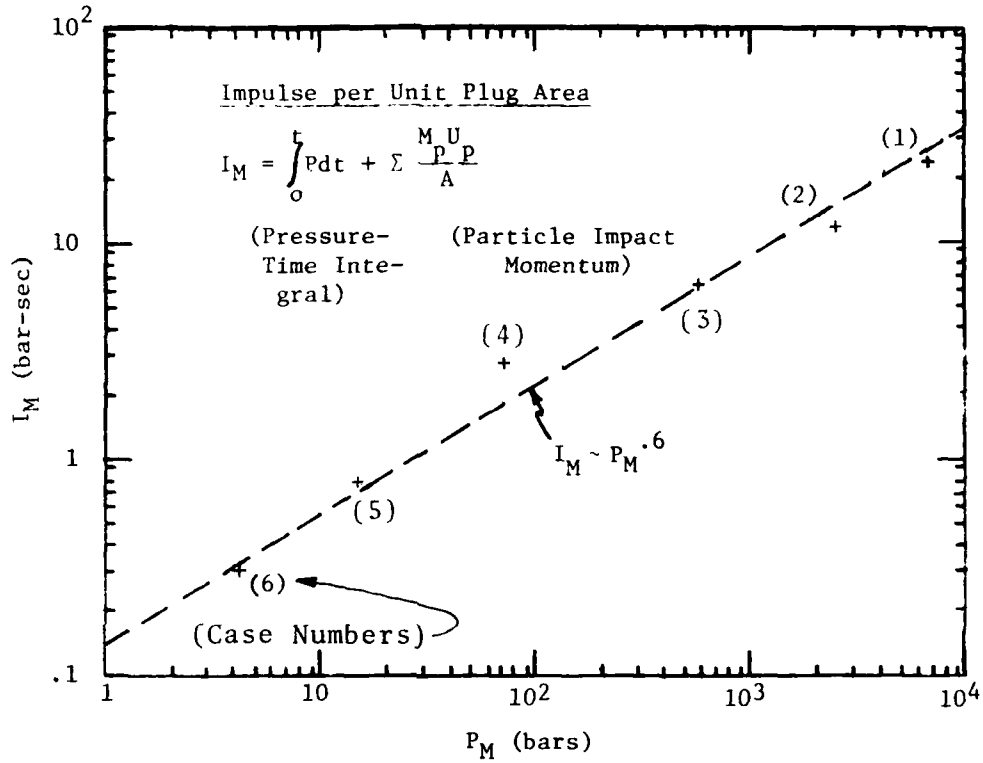

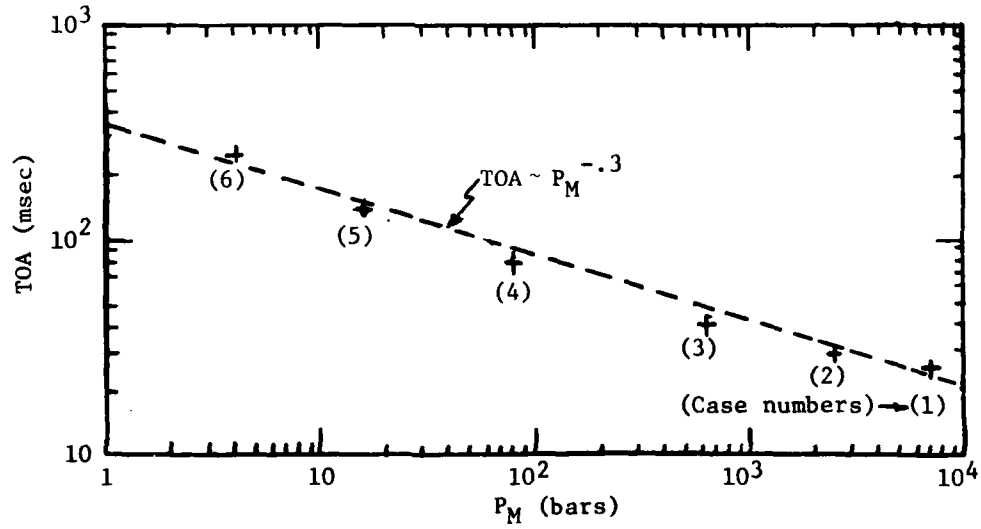

Figure 5. Maximum Impulse (I_M) and Shock Time of Arrival (TOA) versus Maximum Pressure (P_M) at the Plug for Cases 1 through 6 (see Table 1).

relationships in that they indicate debris uncertainties which lead to factors of 10 variations in P_M produce only factors of ~4 uncertainty in I_M.

The *time-resolved* pressures on the plug and the cumulative impulse delivered to the plug are shown in Figure 6 for two cases. Cases 2 and 5 differ in the treatment of the 108 feet behind the shock front. When a ramp dependence for $\beta(x)$ (Case 5) is used in place of a delayed step function (Case 2) the following related effects are observed:

- the maximum pressure is reduced by a factor of ~150.
- the total impulse delivered to the plug is reduced by a factor of ~15.
- the time of arrival increases by a factor of ~4 to 5.
- the duration of the pressure pulse on the plug increases by a factor of ~4 to 5.

Figure 2 summarizes the sensitivity of the pressure loading to variations in the wall debris entrainment rate parameter $\beta(x)$. The pressure-time histories have been shifted to begin at the times of arrival in Table 1. The important effects (~ factor of 40 in P_M) of an order of magnitude change in $\beta=\dot{T}/U_g$ can be seen by comparing Case 3 ($\bar{\beta} = 10^{-4}$) and Case 5 ($\bar{\beta} = 10^{-3}$). Similarly, the effects (~ factor of 4) of reducing the mixing length L by a factor of 2 can be appreciated by comparing Case 5 (L=108 feet) to Case 6 (L=54 feet). *The plug loading characteristics* (P vs time, P_M, and I_M) *are all sensitive to the entrainment of wall debris material near the shock front.*

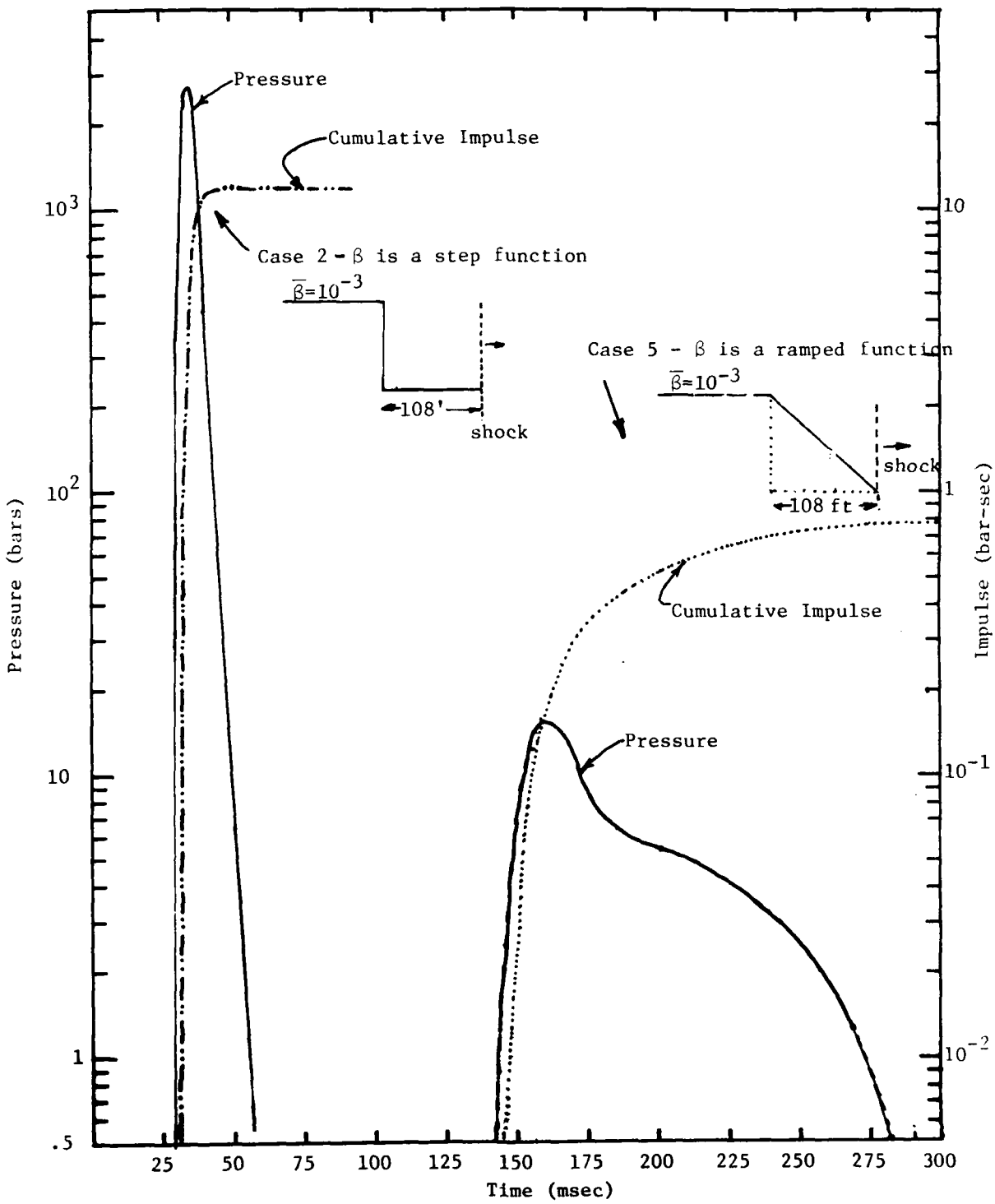

Figure 6. A Comparison of Pressure and Impulse Time Histories using Two Wall Debris Entrainment Models. (Plug is Located 1800 ft from a 1 Mton On-Line Surface Burst.)

3.2 EFFECTS OF PARTICLE SIZE

The multi-phase mixture of air, solid-liquid debris particles, and debris vapor interacts through drag and thermal mechanisms. The drag forces act on both the air and debris; these forces generally accelerate the debris material while decelerating the high velocity air. The thermal interactions involve exchanges of energy primarily through ablation. Both drag and thermal interactions are a strong function of solid/liquid *particle size*.

The influence of uncertainties in the particle size distribution is shown on Figure 7. The only difference between the two numerical simulations is that Case 7 uses a single debris particle size of $D = 100\mu = .01$ cm as compared to the nominal particle size distribution of $D = .1$, 1, and 10 cm particles* used in Case 3.

Figure 7 shows that if wall debris is assumed to mix with the shocked air in "small" particles ($D = 100\mu = .01$ cm), as compared to the nominal particle size distribution ($D = .1$, 1, and 10 cm), then the enhanced drag and thermal interactions will cause the maximum pressure to drop by an additional factor of ~5, and the impulse to drop by an additional factor of ~2.

In order to evaluate the relative importance of drag as compared to thermal interactions, two numerical simulations (Cases 8 and 9) were performed which ignored all thermal mechanisms, i.e. no ablation or conduction was allowed (similar to Cases 3 and 7 on Figure 7 except there are no thermal interactions). Table 2 summarizes the results of these numerical simulations.

---

* In the nominal case, the mass is initially divided equally among each particle size group, i.e 1/3 of the mass is in .1 cm particles, 1/3 in 1 cm particles, and 1/3 in 10 cm particles. This nominal particle size distribution is used in all cases except Cases 7 and 9.

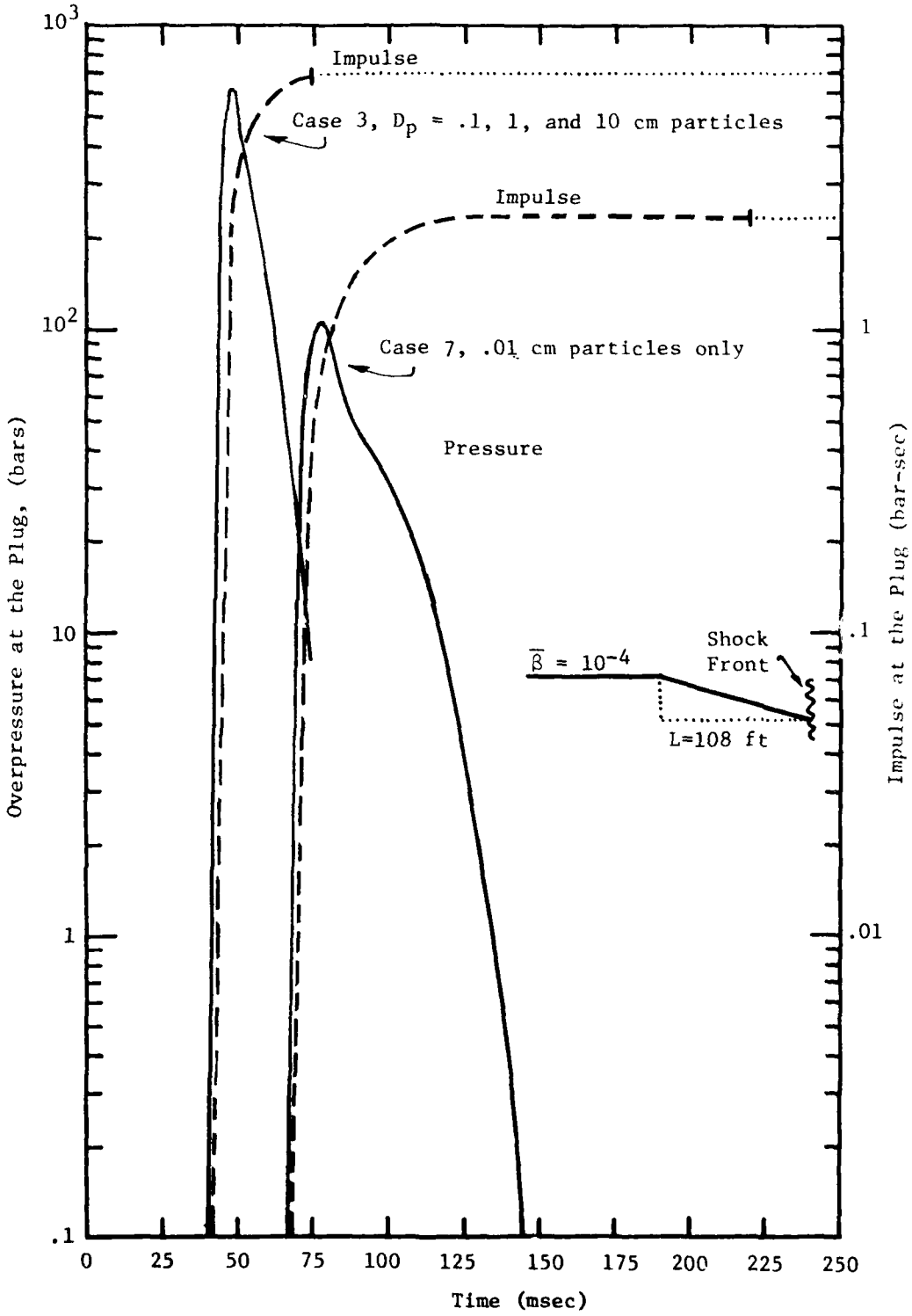

Figure 7. Time Histories of Pressure Delivered to the Plug and Impulse for Variations in the Particle Size Distribution ($\bar{\beta}=10^{-4}$ and L=108 ft using a ramped loading function).

TABLE 2. Maximum Pressures and Impulses Delivered to the Plug for Variations in Particle Size Distribution and Thermal Interaction

Case	Thermal Model Active?	Particle Size Distribution D_p (cm)	Maximum Pressure P_M	Maximum Impulse I_M
3	Yes	.1, 1, and 10*	621	6.4
7	Yes	.01	107	2.4
8	No	.1, 1, and 10*	690	6.9
9	No	.01	136	3.7

* Mass is divided equally among .1, 1, and 10 cm particles in these cases.

Table 2 indicates that the in-trench mixed phase flow dynamics are dominated by drag interactions as opposed to thermal interactions. The maximum pressure is changed by a factor of only ~1.2 when the thermal model is turned off and the initial particle size distribution is held constant (compare Case 3 to Case 8 and Case 7 to Case 9). Thus, the entrained wall debris *mass and particle size distributions* are important in determining the plug loading characteristics (P_M, I_M).

SECTION IV

IN-TRENCH RESPONSE

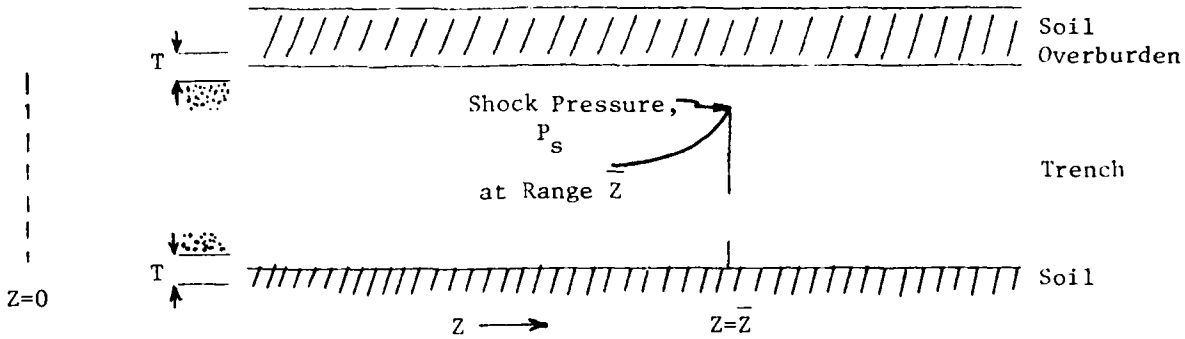

T = wall recession caused by debris becoming entrained in the air flow

Z= In-trench distance from burst

4.1 SHOCK PRESSURE ATTENUATION

The shock pressure attenuation curves are obtained from the numerical simulations by plotting the shock pressure and associated range at a series of times, as sketch below:

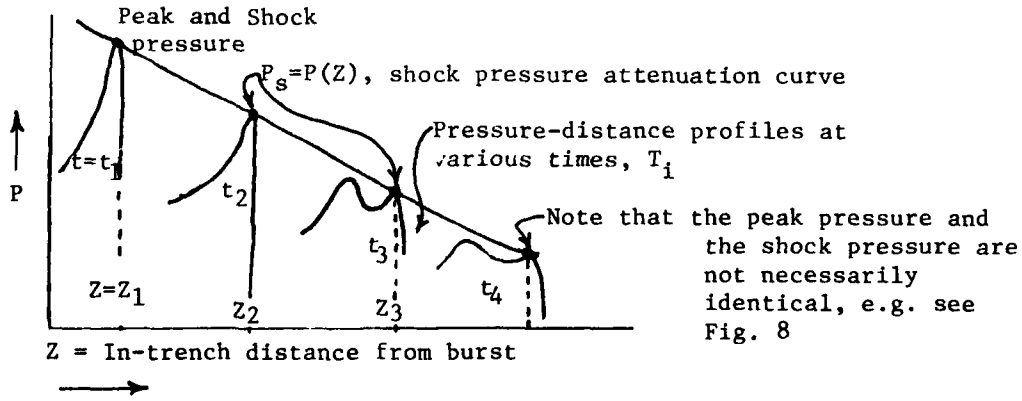

Figure 8 shows the shock pressure attenuation curves and examples of predicted pressure profiles for two debris entrainment lengths of L = 18 feet and 108 feet using a step entrainment function with $\overline{\beta} = 10^{-3}$ (Case 10 vs Case 2). Note that the attenuation in the two cases is very different. Also, the qualitative nature of the pressure profiles is different. When L = 18 feet, the additional entrained mass near the shock front causes the *peak* pressure to (1) decay much more rapidly as compared to the L = 108 feet case, and (2) occur behind the shock front.

Figure 9 shows the effect of varying the mass loading rate parameter, $\overline{\beta}$, for the step entrainment function with L = 18 feet. This figure shows the shock pressure attenuation curves for $\overline{\beta}$ = .01, .001, and .0001.

Figure 10 indicates the effect of wall debris *particle size* on the shock pressure attenuation characteristics. In most of the cases performed in this study, the wall debris was assumed to enter the air flow with 1 mm, 1 cm, and 10 cm particle diameters. The three sizes were evenly distributed according to mass; however, on Figure 10, two cases are shown where the wall debris was assumed to consist of only 100 micron (.01 cm) particles. As Figure 10 shows, the 100 micron particles are very effective in attenuating the shock pressures; this attenuation is primarily due to particle-air drag interactions. Thus, "fast" mixing of small particles with the shock air will be effective in attenuating the shock pressures in the trench.

4.2 WALL RECESSION

Figure 11 shows two comparisons of wall recession thickness versus distance profiles. In the upper portion of this figure, (Figure 11a) the wall recession versus distance profiles are compared for $\overline{\beta} = 10^{-3}$ and $\overline{\beta} = 10^{-4}$ with a step entrainment

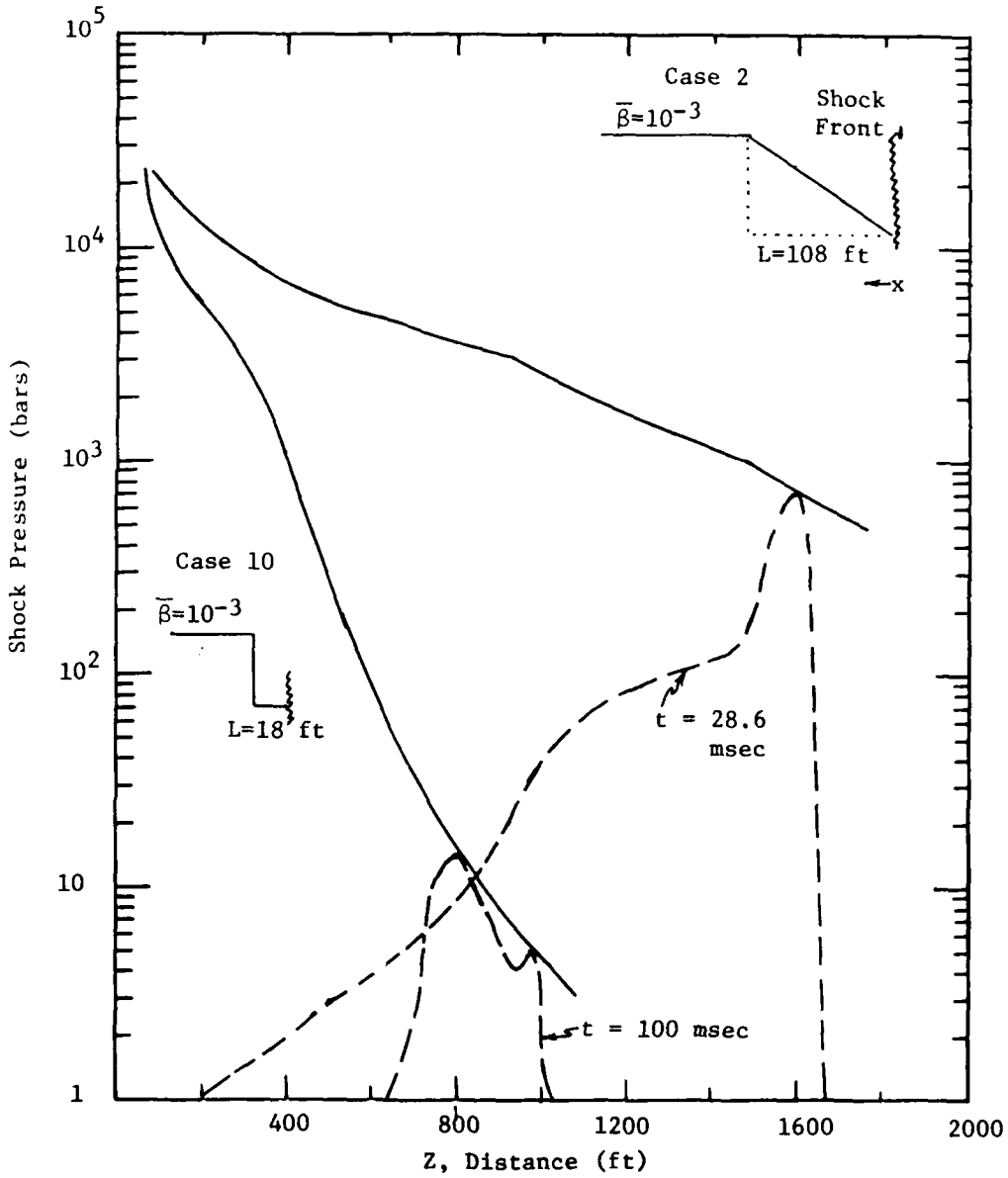

Figure 8. Shock Pressure vs Distance Attenuation Curves for the L =18 ft (Case 10) and L=108 ft (Case 2) Cases Using a Step Entrainment Function with $\bar{\beta}=10^{-3}$. (Dashed curves are Pressure vs Distance Profiles at indicated times.)

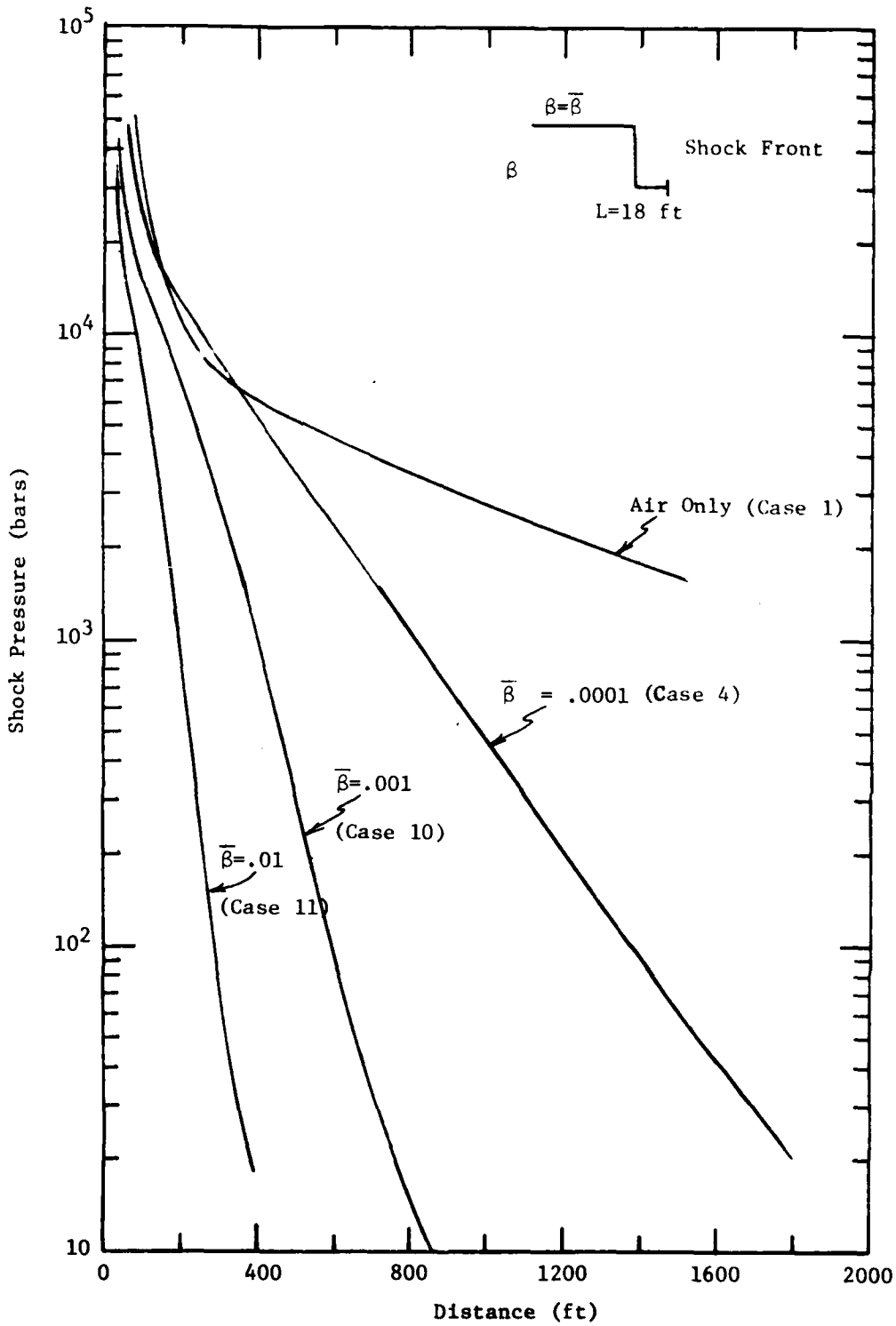

Figure 9. Shock Pressure vs Distance for Various Wall Debris Entrainment Parameters, $\bar{\beta}$=.01, .001, and .0001 (L=18 ft, β is a step function).

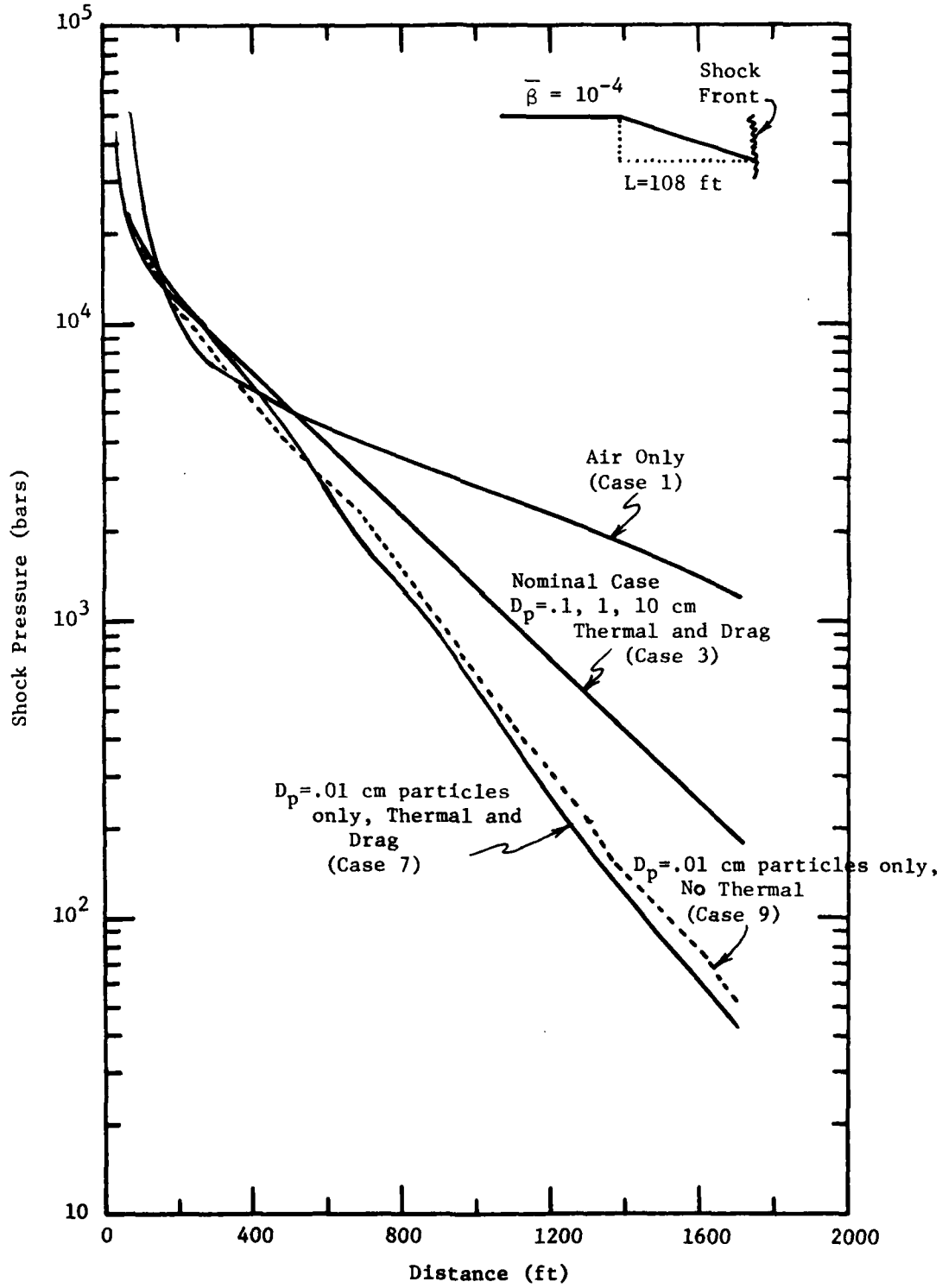

Figure 10. Shock Pressure Attenuation with Distance for Variations in Entrained Particle Size Distribution ($\bar{\beta}=10^{-4}$ and L=108 ft using a Ramped Loading Function).

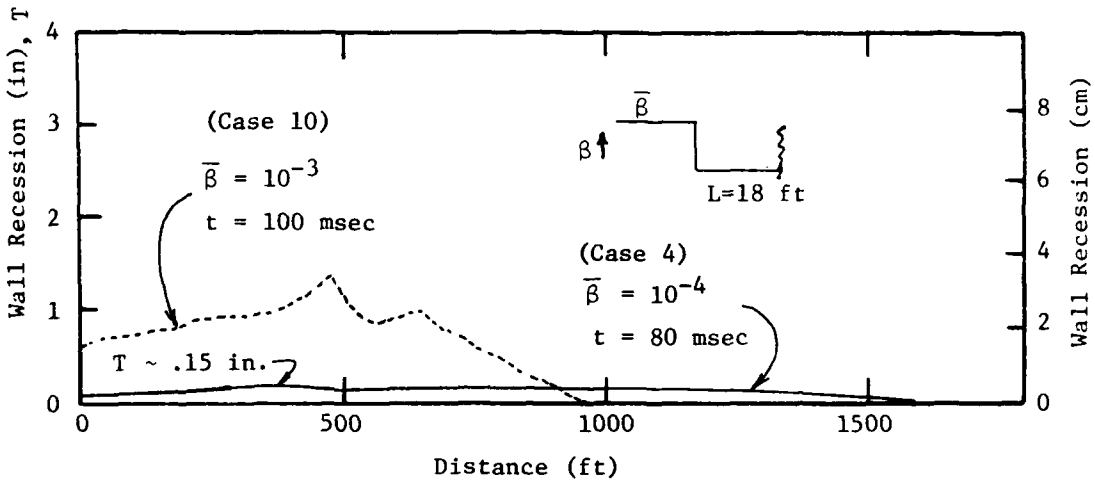

Figure 11a. Wall Recession vs Distance Profiles for $\bar{\beta} = 10^{-3}$ and $\bar{\beta} = 10^{-4}$ (L=18 feet with Step Loading Function).

(Note Change in Scale)

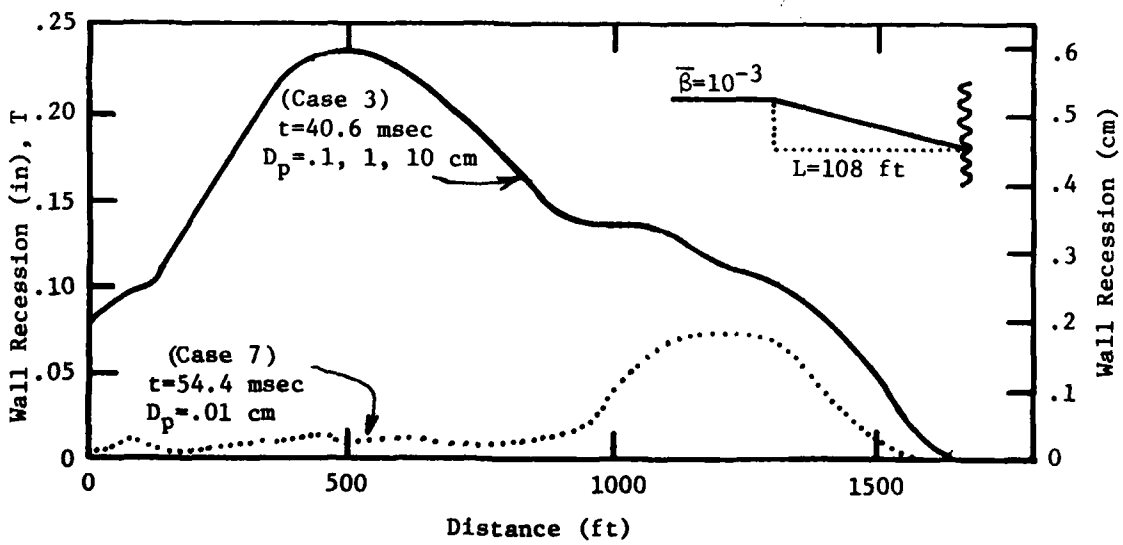

Figure 11b. Wall Recession vs Distance Profiles with Entrained Particle Distributions of D_p = .01 cm and D_p=.1, 1, 10 cm ($\bar{\beta}$=10^{-4} and L=108 ft with Linear Loading Function).

function and L=18 feet. Note that even the fraction of an inch recession (T~.15 in.) in the $\bar{\beta} = 10^{-4}$ case (Case 4) causes the maximum pressure at the plug to drop to 80 bars as compared to the ~6800 bars in the air-only case (Case 1).

Figure 11b compares the wall recession profiles for a variation in debris particle size (Case 7 vs 3). In Case 7, the wall debris particle diameters are entirely 100 microns = .01 cm. In Case 3, the nominal particle size distribution of D_p = .1, 1, and 10 cm is used for the entrained wall debris. Note that in the 100 micron case, <u>less</u> mass has been scoured off the walls, but the attenuation with distance is greater, as previously shown on Figure 10.

APPENDIX A

PHYSICAL MODELS USED IN 1½-D DICE CALCULATIONS

A 1½-D calculation can be used to simulate a flow problem that satisfies two conditions:

1. There is a "well-defined" principal flow direction.
2. Transfer of mass, momentum, and energy transverse to the principal flow direction can be modeled so that numerical integrations are only performed in the principal flow direction.

Within the context of the present parametric analyses of mixed phase flow in trenches, these conditions are adequately satisfied during most of the in-trench flow dynamics. These conditions are not satisfied, however, when the trench roof displacement approaches the trench radius in size. Therefore, the 1½-D analyses are probably poor simulations near the burst point.

The physical models described in this section are of two types:

1. General Physical Models
   - Drag Model
   - Heat Exchange Model
2. Models for Treating Effects of Transverse Flow Interactions.
   - Venting Model
   - Wall Expansion Model

   (The debris entrainment model, which falls in this group, is described in Section II of the text.)

A.1 AERODYNAMIC DRAG

In DICE mixed phase flow calculations, the dirt particles and air experience mutual drag interactions. The basic model used for the DICE drag interaction force (F_D) on a particle of diameter (D_p) moving with velocity ($\vec{V}_p$) in a gas stream of density (ρ_g) and velocity ($\vec{V}_g$) is:

$$F_D = \tfrac{1}{2}\rho_g \, (\vec{V}_p - \vec{V}_g) \, | \, \vec{V}_p - \vec{V}_g \, | \, C_D \left(\frac{\pi D_p^{\,2}}{4}\right) \qquad (A.1)$$

where the drag coefficient (C_D) is defined by:

$$C_D = 0.6 + \frac{36}{Re} \qquad (A.2)$$

and Re is the particle Reynold's number,

$$Re = \frac{D_p \, | \, \vec{V}_p - \vec{V}_g \, | \, \rho_g}{\mu} \qquad (A.3)$$

where

$$\mu = (2.42T)^{0.78} \times 10^{-6} \text{ poise, T in } ^\circ\text{K}$$

The relative masses of particles and gas in a computational cell are used to guarantee that changes in the dirt particle momentum are compensated by oppositely-directed changes in the air momentum (see Reference 2 for additional details).

A.2 THERMAL INTERACTION

The DICE thermal interaction model couples dirt particle ablation, condensation, and internal heat conduction with changes in the air internal energy. Energy is exchanged between the gas phase (air and dirt vapor) and condensed dirt particles by black body radiation and convection. The convective exchange model

includes the effects of the strong radial gas flow that accompanies small particle ablation or condensation. For a complete discussion of the DICE thermal interaction model, refer to Appendix C of Reference 4.

Sample radiative and convective extinction times for dirt particles at a gas temperature of 20,000°K (also assuming P=1 kbar, $Re=10^4$, and a small dirt to air mass ratio) are shown in Figure 12. An extinction time is the time required for a dirt particle of a given initial diameter to ablate completely at constant gas temperature. Observe that the convective extinction time varies as the square of the particle diameter while the radiative extinction time varies as the particle diameter. Thus the 100μ particles have radiative extinction times of about 300 μsec as compared to 3 msec for 1 mm particles.

A.3 1½-D VENTING AND WALL EXPANSION

Roof venting and trench wall expansion are coupled in the 1½-D DICE solutions. An equivalent square trench is defined as shown in Figure 13, parts a and b. The width (W) of a square trench equivalent in cross-sectional area to a cylindrical trench of radius (R_o) is defined by

$$W = \sqrt{\pi}\, R_o \tag{A.4}$$

H is the combined roof and overburden thickness of mean density (ρ_s).

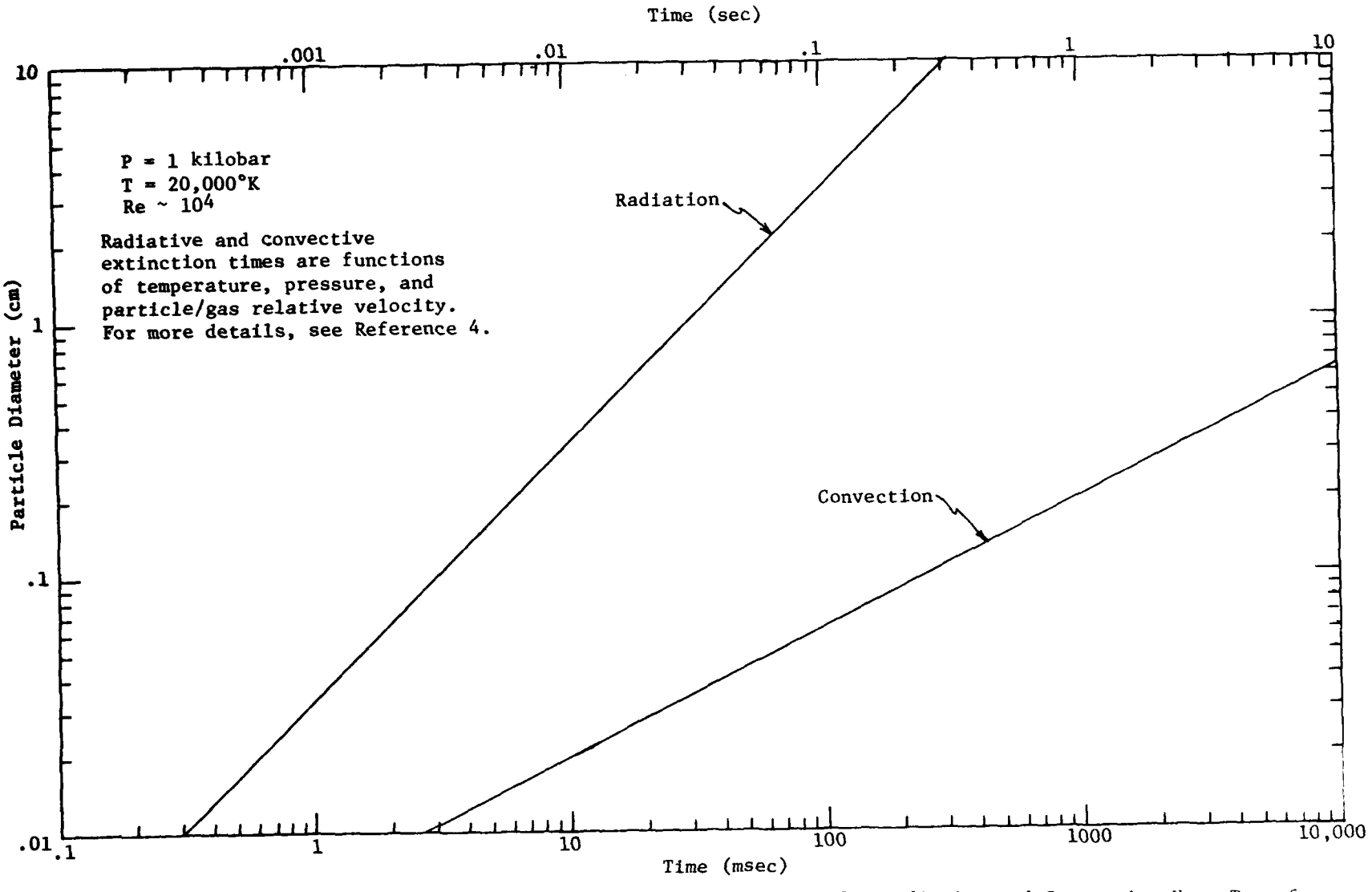

Figure 12. Extinction Times **versus** Particle Diameter for Radiative and Convective Heat Transfer Assuming a Small Dirt to Air Mass Ratio.

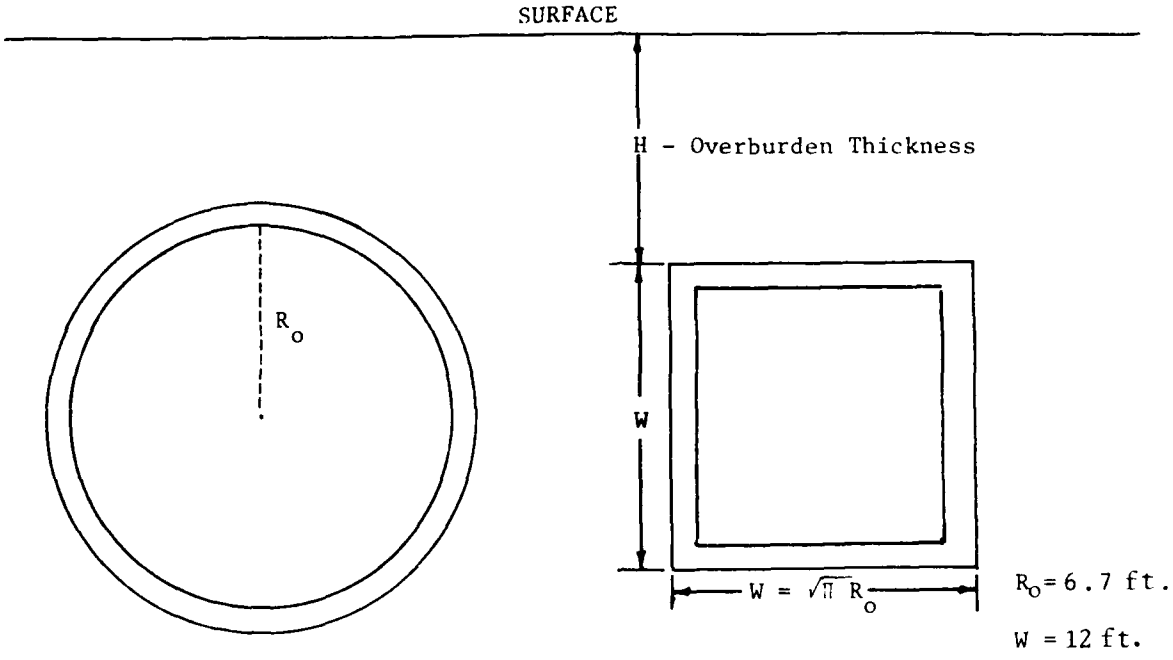

Figure 13a. Equivalence of Circular and Square Trench Crossections

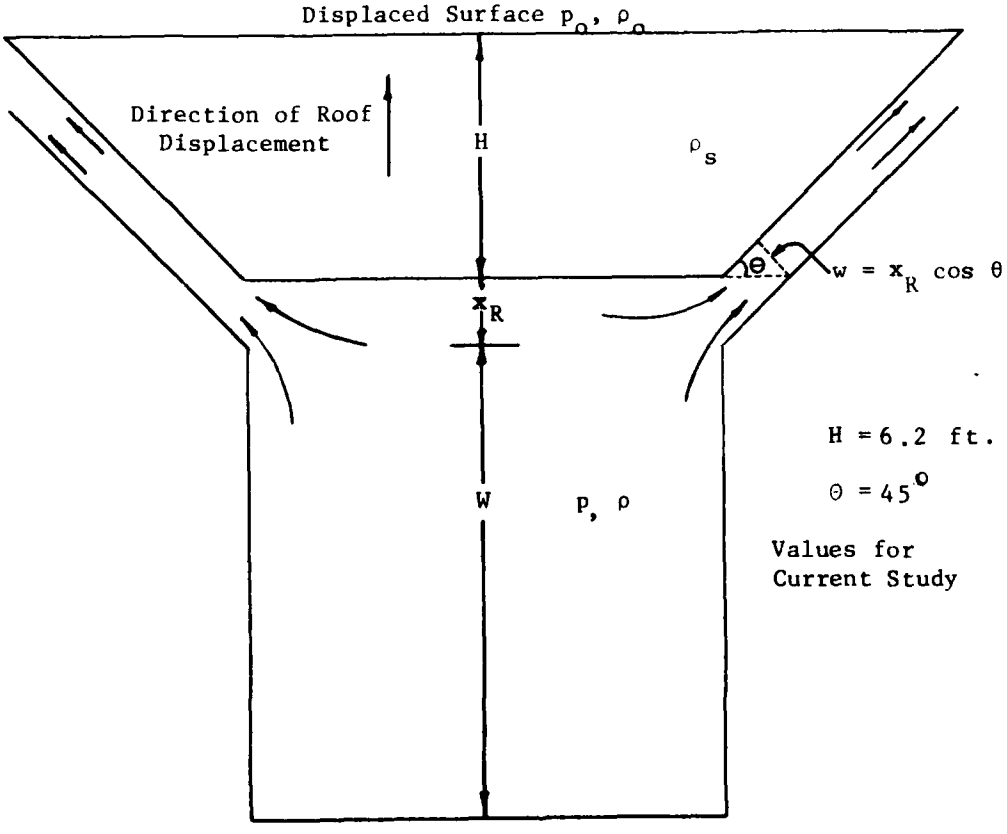

Figure 13b. Wall Expansion and Venting of Equivalent Square Trench

The models assume that the roof displaces upward (with rigid body displacement x_R) as a trapezoidal wedge and that the trench gases vent through the resulting channel of width (w). The moving roof obeys the simple equation of motion.

$$\ddot{x}_R = \frac{p-p_o}{\rho_s H} \tag{A.5}$$

If p is constant during an integration cycle, the roof velocity and displacement are:

$$\dot{x}_R = \frac{(p-p_o)}{\rho_s H} t + \dot{x}_{R_o} \tag{A.6}$$

$$x_R = \frac{(p-p_o)}{2\rho_s H} t^2 + \dot{x}_{R_o} t + x_{R_o} \tag{A.7}$$

where $\dot{x}_{R_o}$ and x_{R_o} are the roof velocity and displacement at the beginning of the integration cycle.

The trench is modeled as completely open when the vent channel area equals the trench roof area or when

$$x_R = W/2\cos\theta \tag{A.8}$$

Prompt venting is assumed to occur for all non-zero values of x_R.

The vent fraction (η) is defined as the ratio of vent area to equivalent square trench roof area,

$$\eta = 2x_R\cos\theta/W \tag{A.9}$$

The venting velocity (V_o) is standardly (Reference 5) defined by

$$V_o = \eta G \left[\frac{2(p-p_o)}{\rho}\right]^{\frac{1}{2}} \qquad (A.10)$$

where G is the ventiliation coefficient (G = .711) and ρ is the trench gas density.

The mass outflow rate per unit length ($\dot{m}_o$) is

$$\dot{m}_o = \rho V_o w = \frac{4Gx_R^2\cos^2\theta}{W}\left[2(p-p_o)\rho\right]^{\frac{1}{2}} \qquad (A.11)$$

If the venting velocity exceeds the local trench sound speed (c), the venting flow is assumed to choke at speed c. In this case

$$\dot{m}_o = \rho c w = 2\rho c x_R \cos\dot{\theta}, \; V_o > c \qquad (A.12)$$

The radius (R) of an expanding cylindrical tunnel was modeled by letting

$$R^2 = R_o^{\,2}\left(1+\frac{x_R}{W}\right) \qquad (A.13)$$

The change in total gas density in the trench due to venting and wall expansion can then be expressed by

$$\dot{\rho} = \dot{\rho}'_{vent} + \dot{\rho}'_{expansion} \qquad (A.14)$$

where

$$\dot{\rho}'_{vent} = -\frac{\dot{m}_o}{\pi R^2} \qquad (A.15)$$

and

$$\dot{\rho}'_{expansion} = -\frac{2\rho\dot{R}}{R} \qquad (A.16)$$

REFERENCES

1. "MX Weapon Systems Concept Validation Phase Survivability Program Plan," Prepared by the Department of the Air Force Space and Missile System Organization (SAMSO) Deputy for Intercontinental Ballistic Missiles, Norton AFB, CA, September 1976.

2. M. Rosenblatt, G. E. Eggum, March 1973, Private Communication.

3. M. Rosenblatt, G. E. Eggum, May 1975, Private Communication.

4. M. Rosenblatt, G. Carpenter and G. Eggum, Sept. 1975, Private Communication.

5. L. M. Milne-Thomson, "Theoretical Hydrodynamics," MacMillan, 1965.

DISTRIBUTION LIST

DEPARTMENT OF DEFENSE

Assistant to the Secretary of Defense
Atomic Energy
ATTN: Executive Assistant

Defense Advanced Rsch. Proj. Agency
ATTN: TIO

Defense Intelligence Agency
ATTN: RDS-3A

Defense Nuclear Agency
ATTN: DDST
ATTN: SPSS, G. Ullrich
ATTN: SPSS, E. Sevin
3 cy ATTN: SPSS, J. Galloway
4 cy ATTN: TITL

Defense Technical Information Center
12 cy ATTN: DD

Field Command
Defense Nuclear Agency
ATTN: FCTMD
ATTN: FCPR

Field Command
Defense Nuclear Agency
Livermore Division
ATTN: FCPRL

Joint Strat. Tgt. Planning Staff
ATTN: XPFS
ATTN: NRI-STINFO Library

Undersecretary of Def. for Rsch. & Engrg.
ATTN: Strategic & Space Systems (OS)

DEPARTMENT OF THE ARMY

BMD Advanced Technology Center
Department of the Army
ATTN: ATC-T

Chief of Engineers
Department of the Army
ATTN: DAEN-RDM
ATTN: DAEN-RDL
ATTN: DAEN-MPE-T, D. Reynolds
ATTN: DAEN-ASI-L

Harry Diamond Laboratories
Department of the Army
ATTN: DELHD-N-P
ATTN: DELHD-I-TL

U.S. Army Ballistic Research Labs.
ATTN: DRDAR-BLE, J. Keefer
ATTN: DRDAR-TSB-S

U.S. Army Cold Region Res. Engr. Lab
ATTN: Library

U.S. Army Construction Engrg. Res. Lab.
ATTN: Library

DEPARTMENT OF THE ARMY (Continued)

U.S. Army Engineer Center
ATTN: Technical Library

U.S. Army Engr. Waterways Exper. Station
ATTN: WESSD, G. Jackson
ATTN: Library
ATTN: WESSA, W. Flathau

U.S. Army Material & Mechanics Rsch. Ctr.
ATTN: Technical Library

U.S. Army Materiel Dev. & Readiness Cmd.
ATTN: DRXAM-TL

U.S. Army Nuclear & Chemical Agency
ATTN: Library

DEPARTMENT OF THE NAVY

Naval Construction Battalion Center
Civil Engineering Laboratory
ATTN: Code L51, J. Crawford
ATTN: Code L08A
ATTN: Code L53, J. Forrest

Naval Facilities Engineering Command
ATTN: Code 09M22C

Naval Postgraduate School
ATTN: Code 0142
ATTN: G. Lindsay

Naval Research Laboratory
ATTN: Code 2627

Naval Surface Weapons Center
ATTN: Code X211
ATTN: Code F31

Naval Surface Weapons Center
ATTN: Tech. Library & Info. Services Branch

Office of Naval Research
ATTN: Code 715

DEPARTMENT OF THE AIR FORCE

Air Force Institute of Technology
Air University
ATTN: Library

Headquarters
Air Force Systems Command
ATTN: DLWM

Air Force Weapons Laboratory, AFSC
ATTN: NT, D. Payton
ATTN: DE, M. Plamondon
ATTN: DED-I
ATTN: DED-A
ATTN: SUL
ATTN: DES-S
ATTN: DES-G
ATTN: DEO
ATTN: DEY

DEPARTMENT OF THE AIR FORCE (Continued)

Assistant Chief of Staff
Intelligence
Department of the Air Force
ATTN: IN

Assistant Secretary of the AF
Research, Development & Logistics
Department of the Air Force
ATTN: SAFALR/DEP for Strat. & Space Sys.

Ballistic Missile Office
Air Force Systems Command
ATTN: MNNX, W. Crabtree
ATTN: MNNXH, D. Gage

Deputy Chief of Staff
Research, Development & Acq.
Department of the Air Force
ATTN: AFRDQA
ATTN: AFRDPN
ATTN: AFRD-M, L. Montulli
ATTN: AFRDQSM

Strategic Air Command
Department of the Air Force
ATTN: XPFS
ATTN: NRI-STINFO Library

Vela Seismological Center
ATTN: G. Ullrich

OTHER GOVERNMENT AGENCY

Federal Emergency Management Agency
ATTN: Hazard Eval. & Vul. Red. Div., G. Sisson

DEPARTMENT OF ENERGY CONTRACTORS

Lawrence Livermore Laboratory
ATTN: Document Control for D. Glenn

Los Alamos Scientific Laboratory
ATTN: Document Control for C. Keller
ATTN: Document Control for R. Sanford

Sandia Laboratories
ATTN: Document Control for Org. 1250, W. Brown
ATTN: Document Control for A. Chabai

DEPARTMENT OF DEFENSE CONTRACTORS

Acurex Corp.
ATTN: C. Wolf
ATTN: K. Triebes
ATTN: J. Stockton

Aerospace Corp.
ATTN: Technical Information Services
ATTN: H. Mirels

Agbabian Associates
ATTN: M. Agbabian

Applied Theory, Inc.
2 cy ATTN: J. Trulio

Boeing Co.
ATTN: Aerospace Library
ATTN: S. Strack

DEPARTMENT OF DEFENSE CONTRACTORS (Continued)

California Research & Technology, Inc.
ATTN: Library
ATTN: M. Rosenblatt
ATTN: G. Carpenter
ATTN: R. Bilyeu

Civil Systems, Inc.
ATTN: J. Bratton

Civil Systems, Inc.
ATTN: S. Melzer

Erich H. Wang
Civil Engineering Rsch. Fac.
ATTN: J. Kovarna
ATTN: P. Lodde

General Electric Company-TEMPO
ATTN: DASIAC

H-Tech Labs, Inc.
ATTN: B. Hartenbaum

Higgins, Auld & Associates
ATTN: N. Higgins
ATTN: H. Auld

IIT Research Institute
ATTN: Documents Library

J. H. Wiggins Co., Inc.
ATTN: J. Collins

Merritt CASES, Inc.
ATTN: Library

Nathan M. Newmark Consult. Eng. Svcs.
ATTN: N. Newmark
ATTN: W. Hall

Pacific-Sierra Research Corp.
ATTN: H. Brode

Mission Research Corp.
ATTN: C. Longmire
ATTN: G. McCartor

Pacifica Technology
ATTN: Library
ATTN: R. Allen

Physics International Co.
ATTN: Technical Library
ATTN: J. Thomsen
ATTN: F. Sauer

R & D Associates
ATTN: J. Lewis
ATTN: Technical Information Center
ATTN: C. MacDonald
ATTN: R. Port
ATTN: J. Carpenter

Science Applications, Inc.
ATTN: H. Wilson
ATTN: R. Schlaug
ATTN: Technical Library

Science Applications, Inc
ATTN: D. Hove

DEPARTMENT OF DEFENSE CONTRACTORS (Continued)

Science Applications, Inc.
ATTN: B. Chambers III

SRI International
ATTN: G. Abrahamson
ATTN: Library
ATTN: J. Colton

Systems, Science & Software, Inc.
ATTN: Library
ATTN: C. Dismukes
ATTN: K. Pyatt
ATTN: J. Barthel

Systems, Science & Software, Inc.
ATTN: J. Murphy

Systems, Science & Software, Inc.
ATTN: C. Hastings

DEPARTMENT OF DEFENSE CONTRACTORS (Continued)

Systems, Science & Software, Inc.
ATTN: C. Needham

Terra Tek, Inc.
ATTN: Library
ATTN: A. Abou-Sayed

TRW Defense & Space Sys. Group
ATTN: Technical Information Center
ATTN: N. Lipner

TRW Defense & Space Sys. Group
ATTN: G. Hulcher

Weidlinger Assoc., Consulting Engineers
ATTN: I. Sandler

Weidlinger Assoc., Consulting Engineers
ATTN: J. Isenberg